

Surface polaritons on metallic and semiconducting cylinders: A complex angular momentum analysis

Stéphane Ancey,^{1,*} Yves Décanini,^{2,†} Antoine Folacci,^{2,‡} and Paul Gabrielli^{1,§}

¹ UMR CNRS 6134 SPE, Equipe Ondes et Acoustique,

Université de Corse, Faculté des Sciences, Boîte Postale 52, 20250 Corte, France

² UMR CNRS 6134 SPE, Equipe Physique Semi-Classique (et) de la Matière Condensée,

Université de Corse, Faculté des Sciences, Boîte Postale 52, 20250 Corte, France

(Dated: November 19, 2018)

We revisit scattering of electromagnetic waves from metallic and semiconducting cylinders in the framework of complex angular momentum techniques. We prove that “resonant surface polariton modes” are generated by a unique surface wave, i.e. a surface polariton, propagating close to the cylinder surface. This surface polariton corresponds to a particular Regge pole of the S -matrix of the cylinder. From the associated Regge trajectory we can construct semiclassically the spectrum of the complex frequencies of the resonant surface polariton modes which can be considered as Breit-Wigner-type resonances. Furthermore, by taking into account Stokes’ phenomenon, we derive an asymptotic expression for the position in the complex angular momentum plane of the surface polariton Regge pole. We then describe semiclassically the surface polariton and provide analytical expressions for its the dispersion relation and its damping. All these features allow us to consider the photon-cylinder system as a kind of artificial atom where the photon plays the role of the electron. Finally, we briefly discuss the implication of our results for two-dimensional photonic crystals.

PACS numbers: 78.20.-e, 41.20.Jb, 73.20.Mf, 42.25.Fx

I. INTRODUCTION

In recent years, since the work of McGurn and Maradudin¹, there has been a growing interest in the study of photonic crystals containing metallic or semiconducting components. The frequency-dependence of the dielectric function $\epsilon(\omega)$ of these materials, as well as the presence of a frequency range where $\epsilon(\omega) < 0$, lead to new features which do not exist in conventional photonic crystals and which are mainly linked to the presence of surface polaritons (SP’s). With this in mind, we intend to revisit the theory of SP’s propagating close to curved metal-dielectric or semiconductor-dielectric interfaces. In this paper, we will emphasize the case of the circular cylindrical interface. For reviews on photonic crystal physics see Refs. 2,3,4. Among the numerous articles dealing with SP’s in photonic crystals, we refer to Refs. 1,5,6,7,8,9,10,11,12,13, i.e. to a non-exhaustive list of works dealing more particularly with two-dimensional arrays of cylinders of circular cross section for which SP’s may be excited and which are consequently relevant to our study.

SP’s supported by flat metal-dielectric or semiconductor-dielectric interfaces can be easily described from a theoretical point of view and their properties can be obtained from rather elementary calculations involving homogeneous and inhomogeneous plane waves. It should be noted that in this context, an SP is clearly defined as a surface wave propagating close to the interface with an amplitude that decays in an exponential fashion perpendicularly to the interface and into both medium. By contrast, in the presence of cylindrical (this is also true for spherical) interfaces, the corresponding theoretical analysis is a little bit

more complicated (see, for example, Refs. 14,15,16,17): Bessel functions must be introduced and transcendental equations involving them must be numerically solved, for example, in order to understand resonance phenomena associated with SP’s. As a consequence, a clear physical description of scattering of electromagnetic waves from curved metal-dielectric or semiconductor-dielectric interfaces does not still exist. In the scientific literature, this fact sometimes leads to a semantic ambiguity with the expression “surface polaritons” denoting the surface waves propagating close to the interface as well as the resonant electromagnetic modes they generate. In order to avoid such an ambiguity and to distinguish between the two physical phenomena, we shall use the more appropriate expression “resonant surface polariton modes” (RSPM’s) for the latter.

Since the sixties, mainly under the impetus of Nussenzweig, asymptotic (i.e., semiclassical) techniques which use analytic continuation of partial-wave representations (Mie sums) have been developed to understand scattering of electromagnetic waves from dielectric objects. Together these techniques form the complex angular momentum (CAM) method. In electromagnetism, it can be considered as a refinement of ray optics which takes into account “tunneling aspects” of scattering and therefore includes diffractive rays associated with surface waves. Of course, the CAM method is an asymptotic approach and formally it is only valid at length scales “large” compared to the wavelength of the electromagnetic field.

The CAM method originates from the pioneering work of Watson¹⁸ dealing with the propagation and diffraction of radio waves around the earth. It has since been successfully introduced in various domains of physics. The success of the CAM method is mainly due to its ability

to provide a clear description of a given scattering problem by extracting the physical information (linked to the geometrical and diffractive aspects of the scattering process) which is hidden in partial-wave representations and then to semiclassically describe resonance phenomena. Here the dual structure of the S -matrix associated with a given scattering problem plays a crucial role. Indeed, the S -matrix is a function of both the frequency ω and the angular momentum index ℓ . It can be analytically extended into the complex ω -plane as well as into the complex ℓ -plane (CAM plane). Its poles lying in the fourth quadrant of the complex ω -plane are the complex frequencies of the resonant modes. In other words, the behavior of the S -matrix in the complex ω -plane permits us to investigate resonance phenomena. The structure of the S -matrix in the complex ℓ -plane allows us, by using integration contour deformations, Cauchy's Theorem and asymptotic analysis, to provide a semiclassical description of scattering in terms of rays. In that context, the poles of the S -matrix lying in the CAM plane (the so-called Regge poles) are associated with diffraction. Of course, when a connection between these two faces of the S -matrix can be established, resonance aspects of scattering are then semiclassically interpreted. For reviews of the CAM method we refer to the monographs of Newton¹⁹, Nussenzveig²⁰ and Grandy²¹ as well as to references therein for various applications in quantum mechanics, nuclear physics, electromagnetism, optics, acoustics and seismology. For recent applications in more "exotic" contexts, we refer to Refs. 22,23,24 where a CAM analysis of black hole scattering and black hole gravitational radiation is provided and to Ref. 25 where the Aharonov-Bohm effect is considered.

As far as we know, the CAM method has never been used to understand scattering of electromagnetic waves from metallic and semiconducting objects. In fact, because of the frequency-dependence of the dielectric function of metals and semiconductors, the extension of the ideas of Nussenzveig and coworkers²⁰ to such a problem is not quite as obvious as it seems at first sight. In this article, we make some steps in that direction but with a rather modest goal. Indeed, we only consider the scattering of TE waves (H polarization) by a metallic or semiconducting circular cylinder surrounded by a dielectric medium. We limit our study to that case because SP's are not excited in the E -polarization configuration. From the S -matrix of the cylinder, using CAM techniques, we develop a semiclassical description of the scattering aspects linked to SP's. More precisely, we prove that RSPM's are generated by a unique SP propagating close to the cylinder surface. This surface wave is associated with a particular Regge pole of the S -matrix of the cylinder. From the corresponding Regge trajectory, i.e. from the curve traced out in the CAM plane by this Regge pole as a function of the frequency, we can construct semiclassically the spectrum of the complex frequencies of RSPM's which can be considered as Breit-Wigner-type resonances. Furthermore, by carefully taking into ac-

count Stokes phenomenon, we derive an asymptotic expression for the position of the SP Regge pole in the CAM plane and then, we can describe semiclassically the SP. In some sense, our results allow us to consider the photon-cylinder system as an artificial atom: RSPM's are long-lived quasibound states for this atom while the trajectory of the SP which generates them and which is supported by the cylinder surface is a Bohr-Sommerfeld-type orbit.

Our paper is organized as follows. In Section 2, we introduce our notations and we construct the S -matrix of the system. We then discuss the resonant aspects of our problem. In Section 3, by using CAM techniques, we establish the connection between the SP propagating close to the surface cylinder and the associated RSPM's. In Section 4, we describe semiclassically the SP by providing analytic expressions for its dispersion relation and its damping. We then deduce analytic approximations for the excitation frequencies of RSPM's. Finally, in Section 5, we conclude our article by considering some possible extensions of our work and by briefly discussing the implication of our results in the context of two-dimensional photonic crystal physics.

II. EXACT S -MATRIX AND SCATTERING RESONANCES

From now on, we consider the scattering of an electromagnetic wave by a metallic or semiconducting circular cylinder with a frequency-dependent dielectric function $\epsilon_c(\omega)$ which is embedded in a host medium of infinite extent with constant dielectric function ϵ_h (region I). In the usual cylindrical polar coordinate system (ρ, θ, z) the cylinder occupies a region corresponding to the range $0 \leq \rho < a$ (region II). We also assume that the magnetic field \mathbf{H} is parallel to the axis of the cylinder (H polarization) and we choose to treat our problem in a two-dimensional setting, ignoring the z coordinate. Furthermore, in the following, we implicitly assume the time dependence $\exp(-i\omega t)$ for the magnetic field and we shall sometimes use the wave numbers

$$k^I(\omega) = \left(\frac{\omega}{c}\right) \sqrt{\epsilon_h} \quad \text{and} \quad k^{II}(\omega) = \left(\frac{\omega}{c}\right) \sqrt{\epsilon_c(\omega)}. \quad (1)$$

Here c is the velocity of light in vacuum.

As far as the dielectric function of the cylinder is concerned, we assume it presents a Drude-like behavior^{26,27}

$$\epsilon_c(\omega) = \epsilon_\infty \left(1 - \frac{\omega_p^2}{\omega^2}\right), \quad (2)$$

or the ionic crystal behavior^{26,27}

$$\epsilon_c(\omega) = \epsilon_\infty \left(\frac{\omega_L^2 - \omega^2}{\omega_T^2 - \omega^2}\right). \quad (3)$$

In both cases, ϵ_∞ is the high-frequency limit of the dielectric function. In Eq. (2), ω_p is the plasma frequency.

In Eq. (3), ω_T and ω_L respectively denote the transverse-optical-phonon frequency and the longitudinal-optical-phonon frequency. In the first case, SP's follow from the coupling of the electromagnetic wave with the plasma wave and are usually called surface plasmon polaritons. In the second one, SP's follow from the coupling of the electromagnetic wave with the longitudinal and transverse acoustic waves and are usually called surface phonon polaritons. Eq. (2) can be used to describe the dielectric behavior of certain metals and semiconductors (Si, Ge, InSb, ...) while Eq. (3) can be used to investigate the optical properties of other semiconductors such as GaAs.

From Maxwell's equations it is easy to show that the z -component of the magnetic field satisfies the Helmholtz equation

$$\left[\Delta_{\mathbf{x}} + \left(\frac{\omega}{c} \right)^2 \epsilon_c(\omega) \right] H_z^{\text{II}}(\mathbf{x}) = 0 \quad \text{for } 0 \leq \rho < a, \quad (4a)$$

$$\left[\Delta_{\mathbf{x}} + \left(\frac{\omega}{c} \right)^2 \epsilon_h \right] H_z^{\text{I}}(\mathbf{x}) = 0 \quad \text{for } \rho > a, \quad (4b)$$

where $\mathbf{x} = (\rho, \theta)$ and with the Laplacian $\Delta_{\mathbf{x}}$ given, in the polar coordinate system, by

$$\Delta_{\mathbf{x}} = \frac{\partial^2}{\partial \rho^2} + \frac{1}{\rho} \frac{\partial}{\partial \rho} + \frac{1}{\rho^2} \frac{\partial^2}{\partial \theta^2}. \quad (5)$$

Furthermore, from the continuity of the tangential components of the electric and magnetic fields (i.e., of E_θ and H_z) at the interface between regions I and II, it can be shown that the z -component of the magnetic field satisfies for $0 \leq \theta < 2\pi$

$$H_z^{\text{I}}(\rho = a, \theta) = H_z^{\text{II}}(\rho = a, \theta), \quad (6a)$$

$$\frac{1}{\epsilon_h} \frac{\partial H_z^{\text{I}}}{\partial \rho}(\rho = a, \theta) = \frac{1}{\epsilon_c(\omega)} \frac{\partial H_z^{\text{II}}}{\partial \rho}(\rho = a, \theta). \quad (6b)$$

We are first interested in the construction of the S -matrix for the cylinder. Because of the cylindrical symmetry of the scatterer, the S -matrix is diagonal and its elements $S_{\ell\ell'}$ are given by $S_{\ell\ell'} = S_\ell \delta_{\ell\ell'}$. For a given angular momentum index $\ell \in \mathbf{Z}$, the coefficient S_ℓ is obtained from the partial wave $(H_z)_\ell$ solution of the following problem (here we extend, *mutatis mutandis*, the quantum mechanical approach developed in Ref. 28):

(i) $(H_z)_\ell$ satisfies the Helmholtz equation (4),

(ii) $(H_z)_\ell$ satisfies the boundary conditions (6),

(iii) at large distance, $(H_z)_\ell$ has the asymptotic behavior

$$(H_z)_\ell(\rho, \theta) \underset{\rho \rightarrow +\infty}{\sim} \frac{1}{\sqrt{2\pi k^{\text{I}} \rho}} \left(e^{-i(k^{\text{I}} \rho - \ell\pi/2 - \pi/4)} + S_\ell(\omega) e^{i(k^{\text{I}} \rho - \ell\pi/2 - \pi/4)} \right) e^{i\ell\theta}.$$

Outside the cylinder (region I), the solution of (4) is expressible in terms of Bessel functions (see Ref. 29) as a linear combination of $J_\ell(k^{\text{I}} \rho) e^{i\ell\theta}$ and $H_\ell^{(1)}(k^{\text{I}} \rho) e^{i\ell\theta}$. Inside the cylinder (region II), it is proportional to $J_\ell(k^{\text{II}} \rho) e^{i\ell\theta}$. As a consequence, the partial wave $(H_z)_\ell$ solution of (i) and (ii) can be obtained exactly. Then, by using the standard asymptotic behavior of Hankel functions for $x \rightarrow \infty$ (see Ref. 29)

$$H_\ell^{(1)}(x) \sim \sqrt{2/(\pi x)} e^{i(x - \ell\pi/2 - \pi/4)}, \quad (7a)$$

$$H_\ell^{(2)}(x) \sim \sqrt{2/(\pi x)} e^{-i(x - \ell\pi/2 - \pi/4)}, \quad (7b)$$

we find from (iii) the expression of the diagonal elements S_ℓ of the S -matrix. We have

$$S_\ell(\omega) = 1 - 2 \frac{D_\ell^{(1)}(\omega)}{D_\ell(\omega)} \quad (8)$$

where $D_\ell^{(1)}(\omega)$ and $D_\ell(\omega)$ are two 2×2 determinants which are explicitly given by

$$D_\ell^{(1)}(\omega) = k^{\text{II}}(\omega) J'_\ell(k^{\text{I}}(\omega)a) J_\ell(k^{\text{II}}(\omega)a) - k^{\text{I}}(\omega) J_\ell(k^{\text{I}}(\omega)a) J'_\ell(k^{\text{II}}(\omega)a), \quad (9a)$$

$$D_\ell(\omega) = k^{\text{II}}(\omega) H_\ell^{(1)'}(k^{\text{I}}(\omega)a) J_\ell(k^{\text{II}}(\omega)a) - k^{\text{I}}(\omega) H_\ell^{(1)}(k^{\text{I}}(\omega)a) J'_\ell(k^{\text{II}}(\omega)a). \quad (9b)$$

The unitarity of the S -matrix¹⁹, which expresses the energy conservation, can be easily verified from (8) and (9) by using elementary properties of Bessel functions. The reciprocity property¹⁹, which is associated with time-reversal invariance, is also satisfied because S_ℓ is an even function of ℓ .

The S -matrix is of fundamental importance because it contains all the information about the scattering process. Its components appear in the Green functions of the problem, in the scattered field when a plane wave excites the cylinder as well as in both the scattering amplitude and the total scattering cross section. As far as the scattering by a plane wave propagating along the x axis is concerned, the total magnetic field in region I is given by

$$H_z^{\text{I}}(\rho, \theta) = e^{ik^{\text{I}} \rho \cos \theta} + \sum_{\ell=0}^{+\infty} \frac{\gamma_\ell}{2} i^\ell [S_\ell - 1] H_\ell^{(1)}(k^{\text{I}} \rho) \cos(\ell\theta). \quad (10)$$

Here γ_ℓ is the Neumann factor ($\gamma_0 = 1$ and for $\ell \neq 0$, $\gamma_\ell = 2$). The scattering amplitude $f(\omega, \theta)$ is defined from the asymptotic behavior of the total magnetic field by

$$H_z^{\text{I}}(\rho, \theta) \underset{\rho \rightarrow +\infty}{\sim} e^{ik^{\text{I}} \rho \cos \theta} + f(\omega, \theta) \frac{e^{ik^{\text{I}} \rho}}{\sqrt{\rho}}. \quad (11)$$

By using the asymptotic behavior (7a) in Eq. (10), we can write

$$f(\omega, \theta) = \sqrt{\frac{1}{2i\pi k^{\text{I}}(\omega)}} \sum_{\ell=0}^{+\infty} \gamma_\ell [S_\ell(\omega) - 1] \cos(\ell\theta). \quad (12)$$

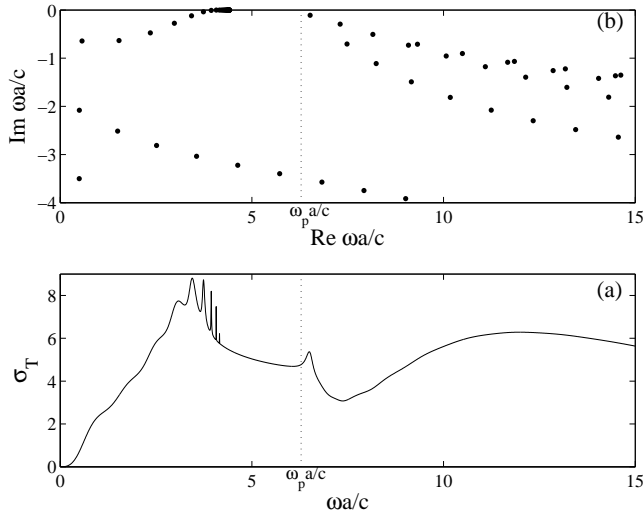


FIG. 1: a) Total cross section σ_T . b) Scattering resonances in the complex $\omega a/c$ -plane. $\epsilon_c(\omega)$ has the Drude type behavior with $\epsilon_\infty = 1$ and $\omega_p a/c = 2\pi$ while $\epsilon_h = 1$.

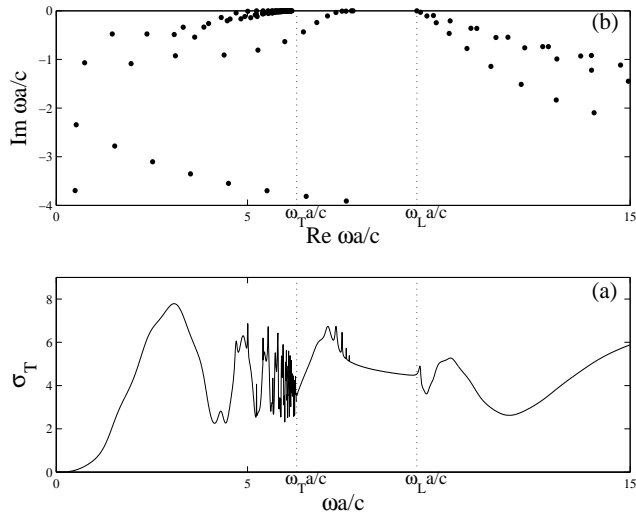


FIG. 2: a) Total cross section σ_T . b) Scattering resonances in the complex $\omega a/c$ -plane. $\epsilon_c(\omega)$ has the ionic crystal behavior with $\epsilon_\infty = 1$, $\omega_T a/c = 2\pi$ and $\omega_L a/c = 3\pi$ while $\epsilon_h = 1$.

Then, the total scattering cross section per unit length of the cylinder can be obtained by using the optical theorem¹⁹:

$$\sigma_T(\omega) = \sqrt{\frac{8\pi}{k^I(\omega)}} \text{Im} \left(e^{-i\pi/4} f(\omega, \theta = 0) \right). \quad (13)$$

In Figs. 1a and 2a, we present two examples of total cross section. They are both plotted as functions of the reduced frequency $\omega a/c$. In Fig. 1a, the cylinder is embedded in vacuum ($\epsilon_h = 1$) and its dielectric function is given by (2) with $\epsilon_\infty = 1$ and $\omega_p a/c = 2\pi$. In Fig. 2a, the cylinder is embedded in vacuum ($\epsilon_h = 1$) and its dielec-

tric function is given by (3) with $\epsilon_\infty = 1$, $\omega_T a/c = 2\pi$ and $\omega_L a/c = 3\pi$. Even if we restrict ourselves to those particular configurations, it should be noted that the results emphasized numerically and that we shall now discuss are very general. On the two figures, rapid variations of sharp characteristic shapes can be observed. This strongly fluctuating behavior is due to scattering resonances. These resonances are the poles of the S -matrix lying in the fourth quadrant of the complex ω -plane and they are determined by solving

$$D_\ell(\omega) = 0 \quad \text{for } \ell \in \mathbb{N}. \quad (14)$$

The solutions of (14) are denoted by $\omega_{\ell p} = \omega_{\ell p}^{(o)} - i\Gamma_{\ell p}/2$ where $\omega_{\ell p}^{(o)} > 0$ and $\Gamma_{\ell p} > 0$, the index p permitting us to distinguish between the different roots of (14) for a given ℓ . In the immediate neighborhood of the resonance $\omega_{\ell p}$, $S_\ell(\omega)$ has the Breit-Wigner form, i.e., is proportional to

$$\frac{\Gamma_{\ell p}/2}{\omega - \omega_{\ell p}^{(o)} + i\Gamma_{\ell p}/2}. \quad (15)$$

As a consequence, when a pole of the S -matrix is sufficiently close to the real axis in the complex ω -plane, it has an appreciable influence on the scattering amplitude and therefore on the total cross section. Of course, if a pole is very close to this axis, the corresponding peak is too sharp to be observed on the total cross section. In Figs. 1b and 2b, resonances are exhibited for the two configurations previously considered. A one-to-one correspondence between the peaks of σ_T and the resonances near the real $\omega a/c$ -axis can be clearly observed in certain frequency ranges.

More precisely and more generally, for the dielectric function (2) there exists in the frequency range $\omega < \omega_p$ where $\epsilon_c(\omega) < 0$ a family of resonances close to the real axis of the complex ω -plane which converges, for large ℓ , to the limiting frequency ω_s satisfying

$$\epsilon_c(\omega_s) + \epsilon_h = 0 \quad (16)$$

and given by

$$\omega_s = \frac{\omega_p}{\sqrt{1 + \epsilon_h/\epsilon_\infty}}. \quad (17)$$

For the dielectric function (3), the same type of behavior occurs but in two different frequency ranges: in the region $\omega < \omega_T$ (here $\epsilon_c(\omega) > 0$) with an accumulation of resonances at the pole ω_T of the dielectric function and in the region $\omega_T < \omega < \omega_L$ (here $\epsilon_c(\omega) < 0$) with an accumulation of resonances at the limiting frequency ω_s still satisfying (16) but which is now given by

$$\omega_s = \sqrt{\frac{\omega_L^2 + (\epsilon_h/\epsilon_\infty)\omega_T^2}{1 + \epsilon_h/\epsilon_\infty}}. \quad (18)$$

We must keep in mind that in the scattering of a H -polarized photon with frequency $\omega_{\ell p}^{(o)}$, a decaying state

of the photon-cylinder system is formed. It has a finite lifetime proportional to $1/\Gamma_{\ell p}$. The resonant states whose complex frequencies belong to one of the families previously described are therefore long-lived states. Because of these particular quasibound states, the photon-cylinder system behaves as a kind of artificial atom for which the photon plays the usual role of the electron. We shall come back to this point of view in the next two sections.

From now on, we shall more particularly focus our attention on the physical interpretation of the long-lived resonant states whose excitation frequencies belong to frequency ranges in which $\epsilon_c(\omega) < 0$. We shall prove that these states are generated by a SP propagating close to the cylinder surface and for this reason we call them RSPM's. For such states, the artificial-atom point of view can be pushed farther as we shall show in Sections 3 and 4. For the long-lived resonant states whose excitation frequencies belong to the frequency range in which $\epsilon_c(\omega) > 0$ (the so-called bulk polariton states), we are not able to provide a similar analysis. This is not very serious as they do not have, in photonic crystal physics, the importance of RSPM's.

III. SEMICLASSICAL ANALYSIS: FROM THE SP REGGE POLE TO THE COMPLEX FREQUENCIES OF RSPM'S

Using the CAM method, we can provide a physical picture of the scattering process in term of diffraction by surface waves and more particularly a physical explanation of the excitation mechanism of RSPM's valid for "high frequencies". By means of a Watson transformation¹⁸ applied to the scattering amplitude (12), we can write

$$f(\omega, \theta) = -\sqrt{\frac{i}{2\pi k^I(\omega)}} \mathcal{P} \int_{\mathcal{C}} \frac{(S_\lambda(\omega) - 1)}{\sin \pi \lambda} \cos[\lambda(\pi - \theta)] d\lambda. \quad (19)$$

Here \mathcal{C} is the integration contour in the complex λ -plane¹⁸ illustrated in Fig. 3 and which encircles the real axis in the clockwise sense. In Eq. (19), \mathcal{P} which stands for Cauchy's principal value at the origin is used in order to reproduce the Neumann factor. The Watson transformation has permitted us to replace the ordinary angular momentum ℓ by the complex angular momentum λ . $S_\lambda(\omega)$ is now an analytic extension of $S_\ell(\omega)$ into the complex λ -plane which is regular in the vicinity of the positive real λ axis. Using Cauchy's theorem and by noting that inside the contour \mathcal{C} , the only singularities of the integrand in (19) are the integers, we can easily recover (12) from (19).

We can then deform the path of integration in (19) taking into account the possible singularities. The only singularities that are encountered are the poles of the S-matrix lying in the CAM plane. They are known as Regge poles^{19,20} and are determined by solving

$$D_\lambda(\omega) = 0 \quad \text{for } \omega > 0. \quad (20)$$

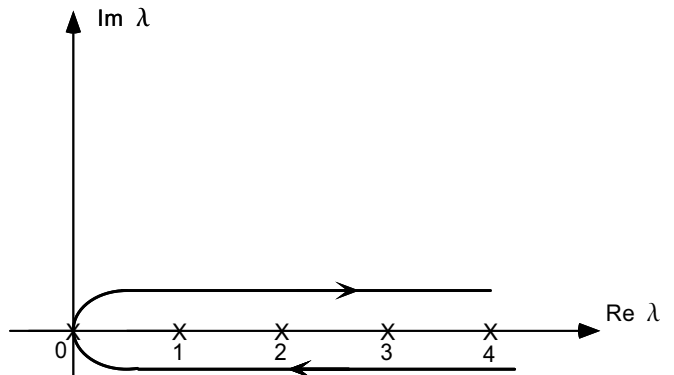


FIG. 3: The Watson integration contour.

Figs. 4 and 5 exhibit the distribution of Regge poles for a cylinder embedded in vacuum. We still consider the two configurations previously studied. We do not display the Regge pole distributions for other configurations (i.e. for other values of the parameters ϵ_∞ , ϵ_h , ω_P , ω_T or ω_L) because they are not really different from those of Figs. 4 and 5. In fact, all these Regge pole distributions are rather similar to the distributions associated with the dielectric objects usually studied²⁰. However, in the frequency range where $\epsilon(\omega) < 0$, something new occurs: it exists a particular Regge pole lying in the first quadrant of the λ -plane and very close to the real axis. It is not present for ordinary dielectric objects. As we shall see below, this new Regge pole is associated with a SP orbiting around metallic or semiconducting cylinders. From now on, we shall denote it by $\lambda_{\text{SP}}(\omega)$.

By Cauchy's theorem we can then extract from (19) the contribution of a residue series over Regge poles. In fact, we limit our study to the contribution of $\lambda_{\text{SP}}(\omega)$ which is given by

$$f_{\text{SP}}(\omega, \theta) = \sqrt{\frac{2\pi}{ik^I(\omega)}} \frac{r_{\text{SP}}(\omega)}{\sin[\pi\lambda_{\text{SP}}(\omega)]} \cos[\lambda_{\text{SP}}(\omega)(\pi - \theta)]. \quad (21)$$

Here $r_{\text{SP}}(\omega) = \text{residue}(S_\lambda(\omega))_{\lambda=\lambda_{\text{SP}}(\omega)}$. Of course, f differs from f_{SP} by a smooth background integral and by the contributions of all other Regge poles. We are not interested by these contributions which do not play any role in the excitation of RSPM's. We think that these contributions could be studied, *mutatis mutandis*, in the framework of CAM techniques developed by Nussenzveig and coworkers²⁰. By using

$$\frac{1}{\sin \pi \lambda} = -2i \sum_{m=0}^{+\infty} e^{i\pi(2m+1)\lambda}$$

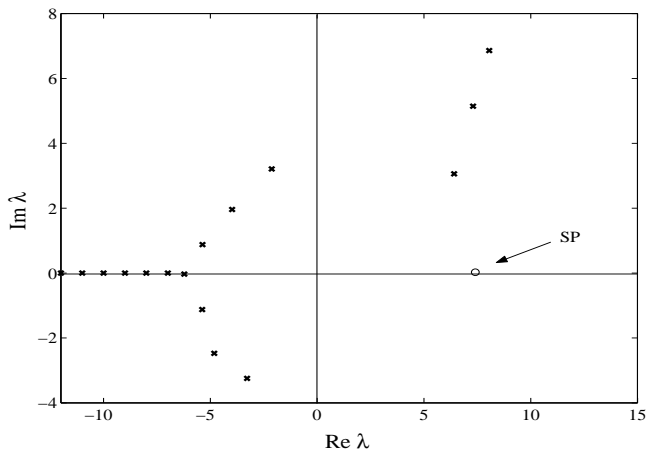


FIG. 4: Regge poles in the complex angular momentum plane. $\epsilon_c(\omega)$ has the Drude type behavior with $\epsilon_\infty = 1$ and $\omega_p a/c = 2\pi$ while $\epsilon_h = 1$. The distribution corresponds to $\omega a/c = 4$.

which is true if $\text{Im } \lambda > 0$, we can write

$$f_{\text{SP}}(\omega, \theta) = -\sqrt{\frac{2i\pi}{k^{\text{I}}(\omega)}} r_{\text{SP}}(\omega) \times \sum_{m=0}^{+\infty} \left(e^{i\lambda_{\text{SP}}(\omega)(\theta+2m\pi)} + e^{i\lambda_{\text{SP}}(\omega)(2\pi-\theta+2m\pi)} \right). \quad (22)$$

In Eq. (22), exponential terms correspond to surface wave contributions. Because the Regge pole $\lambda_{\text{SP}}(\omega)$ lies in the first quadrant of the CAM plane, $\exp[i\lambda_{\text{SP}}(\omega)(\theta)]$ (resp. $\exp[i\lambda_{\text{SP}}(\omega)(2\pi-\theta)]$) corresponds to a surface wave propagating counterclockwise (resp. clockwise) around the cylinder and $\text{Re } \lambda_{\text{SP}}(\omega)$ represents its azimuthal propagation constant while $\text{Im } \lambda_{\text{SP}}(\omega)$ is its damping constant. The exponential decay $\exp[-\text{Im } \lambda_{\text{SP}}(\omega)\theta]$ (resp. $\exp[-\text{Im } \lambda_{\text{SP}}(\omega)(2\pi-\theta)]$) is due to continual re-radiation of energy. Moreover, in (22), the sum over m takes into account the multiple circumnavigations of the surface waves around the cylinder as well as the associated radiation damping. The Regge pole λ_{SP} is very close to the real axis in the complex λ -plane. It then corresponds to a surface wave which is slightly attenuated during its propagation and which contributes significantly to the scattering process and to the resonance mechanism.

As ω varies, the Regge pole $\lambda_{\text{SP}}(\omega)$ describes a Regge trajectory¹⁹ in the CAM plane. In Figs. 6 and 7, we have displayed the Regge trajectories of SP's for the two configurations previously studied. It should be noted that as $\omega \rightarrow \omega_s$, the real part of the SP Regge pole increases indefinitely while its imaginary part vanishes. For other configurations (i.e. for other values of the parameters ϵ_∞ , ϵ_h , ω_p , ω_T or ω_L), we have verified that the SP Regge pole behavior is very similar.

The resonant behavior of the cylinder-photon system

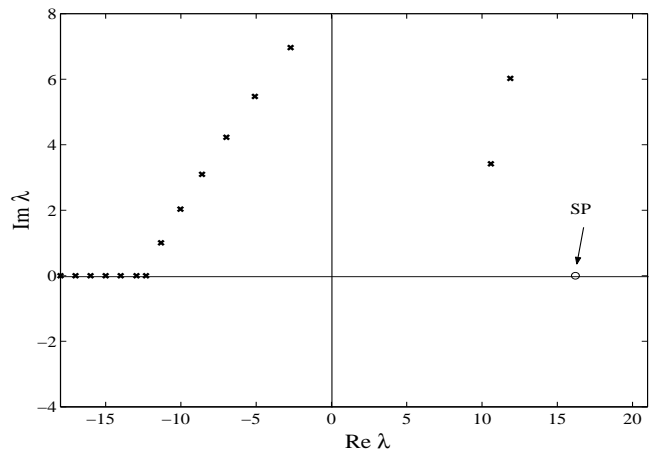


FIG. 5: Regge poles in the complex angular momentum plane. $\epsilon_c(\omega)$ has the ionic crystal behavior with $\epsilon_\infty = 1$, $\omega_T a/c = 2\pi$ and $\omega_L a/c = 3\pi$ while $\epsilon_h = 1$. The distribution corresponds to $\omega a/c = 7.8$.

can now be understood in terms of the Regge trajectory of the SP. When the quantity $\text{Re } \lambda_{\text{SP}}(\omega)$ coincides with an integer, a resonance occurs. Indeed, it is produced by a constructive interference between the different components of the surface wave, each component corresponding to a different number of circumnavigations. Resonance excitation frequencies $\omega_{\ell\text{SP}}^{(o)}$ are therefore obtained from the Bohr-Sommerfeld type quantization condition

$$\text{Re } \lambda_{\text{SP}} \left(\omega_{\ell\text{SP}}^{(o)} \right) = \ell \quad \ell = 0, 1, 2, \dots \quad (23)$$

By assuming that ω is in the neighborhood of $\omega_{\ell\text{SP}}^{(o)}$ and using $\text{Re } \lambda_{\text{SP}}(\omega) \gg \text{Im } \lambda_{\text{SP}}(\omega)$ (which can be numerically verified, except for low frequencies), we can expand $\lambda_{\text{SP}}(\omega)$ in a Taylor series about $\omega_{\ell\text{SP}}^{(o)}$, and obtain

$$\lambda_{\text{SP}}(\omega) \approx \ell + \frac{d\text{Re } \lambda_{\text{SP}}(\omega)}{d\omega} \Big|_{\omega=\omega_{\ell\text{SP}}^{(o)}} (\omega - \omega_{\ell\text{SP}}^{(o)}) + i \text{Im } \lambda_{\text{SP}}(\omega_{\ell\text{SP}}^{(o)}) + \dots \quad (24)$$

Then, by replacing (24) in the term $\cos[\pi\lambda_{\text{SP}}(\omega)]$ of (21), we show that $f_{\text{SP}}(\omega, \theta)$ presents a resonant behavior given by the Breit-Wigner formula (15) with

$$\frac{\Gamma_{\ell\text{SP}}}{2} = \frac{\text{Im } \lambda_{\text{SP}}(\omega)}{d \text{Re } \lambda_{\text{SP}}(\omega)/d\omega} \Big|_{\omega=\omega_{\ell\text{SP}}^{(o)}}. \quad (25)$$

Eqs. (23) and (25) are semiclassical formulas which permit us to determine the location of the resonances from the Regge trajectory of λ_{SP} .

Tables I and II present samples of complex frequencies of RSPM's for the two configurations previously considered. They are calculated from the semiclassical formulas (23) and (25) by using the Regge trajectories numerically determined by solving (20) (see Figs. 6 and 7). A comparison between the “exact” and the semiclassical spectra

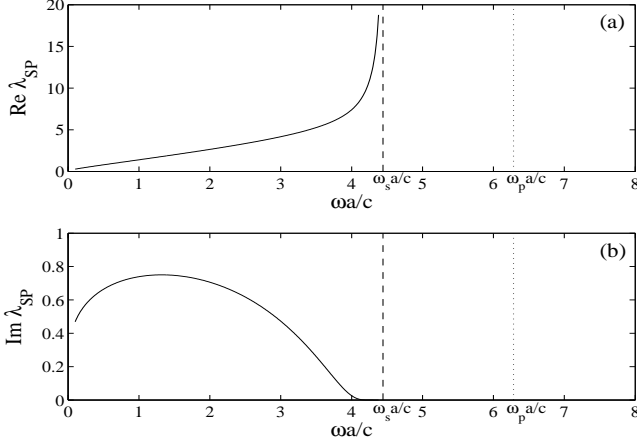


FIG. 6: Regge trajectory for the SP Regge pole. $\epsilon_c(\omega)$ has the Drude type behavior with $\epsilon_\infty = 1$ and $\omega_p a/c = 2\pi$ while $\epsilon_h = 1$. As $\omega a/c \rightarrow \omega_s a/c$, the real part of the SP Regge pole increases indefinitely while its imaginary part vanishes.

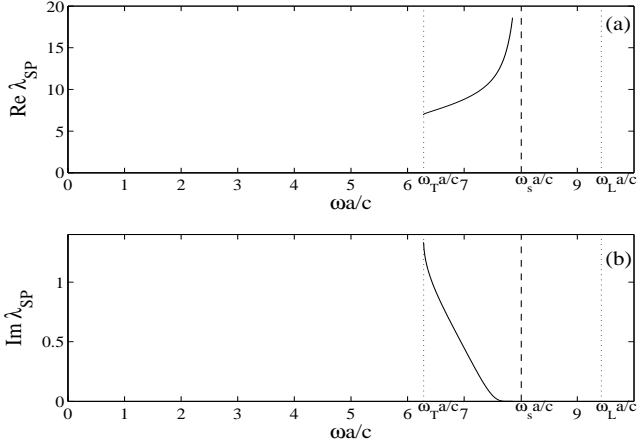


FIG. 7: Regge trajectory for the SP Regge pole. $\epsilon_c(\omega)$ has the ionic crystal behavior with $\epsilon_\infty = 1$, $\omega_T a/c = 2\pi$ and $\omega_L a/c = 3\pi$ while $\epsilon_h = 1$. As $\omega a/c \rightarrow \omega_s a/c$, the real part of the SP Regge pole increases indefinitely while its imaginary part vanishes.

shows a very good agreement, except for “low” frequencies. We have also performed the corresponding calculations for other configurations with $\epsilon_h \neq 1$ and $\epsilon_\infty \neq 1$. The agreement seems even better. Furthermore, inserted into the semiclassical formulas (23) and (25), the behavior of Regge trajectories near the limiting frequencies ω_s easily explains the existence of the families of resonances close to the real axis of the complex ω -plane which converges for large ℓ to the limiting frequency ω_s . In conclusion, we have established a connection between the complex frequencies of RSPM’s and a particular surface wave, the so-called SP, described by a particular Regge pole of the S -matrix and which orbits around the cylinder.

TABLE I: The first complex frequencies of RSPM’s. $\epsilon_c(\omega)$ has the Drude type behavior with $\epsilon_\infty = 1$ and $\omega_p a/c = 2\pi$ while $\epsilon_h = 1$.

ℓ	Exact $\omega_{\ell SP}^{(o)}$	Exact $\Gamma_{\ell SP}/2$	Semiclassical $\omega_{\ell SP}^{(o)}$	Semiclassical $\Gamma_{\ell SP}/2$
1	0.570278	0.642122	0.665828	0.582435
2	1.53524	0.633630	1.49245	0.602114
3	2.35038	0.475286	2.25693	0.476399
4	2.97766	0.274602	2.90439	0.289791
5	3.42645	0.119226	3.39638	0.127238
6	3.73632	0.036765	3.73016	0.037645
7	3.94064	0.007494	3.94009	0.007435
8	4.07049	0.000999	4.07047	0.000981
9	4.15483	0.000093	4.15476	0.000094
10	4.21272	0.000006	4.21266	0.000006

TABLE II: The first complex frequencies of RSPM’s. $\epsilon_c(\omega)$ has the ionic crystal behavior with $\epsilon_\infty = 1$, $\omega_T a/c = 2\pi$ and $\omega_L a/c = 3\pi$ while $\epsilon_h = 1$.

ℓ	Exact $\omega_{\ell SP}^{(o)}$	Exact $\Gamma_{\ell SP}/2$	Semiclassical $\omega_{\ell SP}^{(o)}$	Semiclassical $\Gamma_{\ell SP}/2$
7	6.459387	0.4345112	6.283821	0.0837525
8	6.809183	0.2419456	6.698432	0.3004512
9	7.091176	0.1055079	7.056186	0.1188560
10	7.311233	0.0353546	7.304271	0.0371596
11	7.470835	0.0088275	7.470046	0.0088537
12	7.581710	0.0016441	7.581652	0.0016417
13	7.659584	0.0002366	7.659579	0.0002392
14	7.716557	0.0000273	7.716543	0.0000274
15	7.759919	0.0000026	7.759919	0.0000027

IV. SEMICLASSICAL ANALYSIS: ASYMPTOTICS FOR THE SP AND PHYSICAL DESCRIPTION

A deeper understanding of the SP behavior can be obtained by solving perturbatively Eq. (20) for $\lambda = \lambda_{SP}$. We first replace the Bessel function $J_\lambda(z)$ by the modified Bessel function $I_\lambda(z)$ (see Ref. 29) in order to take into account the fact that $\epsilon_c(\omega) < 0$. Eq. (20) reduces to

$$\frac{1}{\sqrt{\epsilon_h}} \frac{H_{\lambda_{SP}}^{(1)'}(\sqrt{\epsilon_h} a \omega / c)}{H_{\lambda_{SP}}^{(1)}(\sqrt{\epsilon_h} a \omega / c)} = - \frac{1}{\sqrt{-\epsilon_c(\omega)}} \frac{I_{\lambda_{SP}}'(\sqrt{-\epsilon_c(\omega)} a \omega / c)}{I_{\lambda_{SP}}(\sqrt{-\epsilon_c(\omega)} a \omega / c)}. \quad (26)$$

In the right-hand side of (26), we can use the uniform asymptotic expansions of $I_\lambda(z)$ for large orders (see Ref. 29), i.e.

$$I_\lambda(z) \sim \frac{1}{\sqrt{2\pi}} \frac{1}{(\lambda^2 + z^2)^{1/4}} e^{F_\lambda(z)/2} \quad (27)$$

where

$$\frac{F_\lambda(z)}{2} = (\lambda^2 + z^2)^{1/2} + \lambda \ln \left(\frac{z}{\lambda + (\lambda^2 + z^2)^{1/2}} \right). \quad (28)$$

By assuming $|\lambda_{\text{SP}}| \gg \sqrt{-\epsilon_c(\omega)}a\omega/c$, we then obtain

$$-\frac{1}{\sqrt{-\epsilon_c(\omega)}} \frac{I'_{\lambda_{\text{SP}}}(\sqrt{-\epsilon_c(\omega)}a\omega/c)}{I_{\lambda_{\text{SP}}}(\sqrt{-\epsilon_c(\omega)}a\omega/c)} \sim \frac{[\lambda_{\text{SP}}^2 - \epsilon_c(\omega)(a\omega/c)^2]^{1/2}}{\epsilon_c(\omega)(a\omega/c)}. \quad (29)$$

In the left-hand side of (26), the relative positions of λ_{SP} and $\sqrt{\epsilon_h}a\omega/c$ in the λ -complex plane (see Fig. 10) permit us to employ the Debye asymptotic expansion of $H_{\lambda}^{(1)}(z)$ in the form^{30,31}

$$H_{\lambda}^{(1)}(z) \sim -iA(\lambda, z)e^{-\alpha(\lambda, z)} \quad (30)$$

where

$$A(\lambda, z) = \left(\frac{2}{\pi}\right)^{1/2} (\lambda^2 - z^2)^{-1/4}, \quad (31a)$$

$$\alpha(\lambda, z) = (\lambda^2 - z^2)^{1/2} - \lambda \ln\left(\frac{z + (\lambda^2 - z^2)^{1/2}}{z}\right). \quad (31b)$$

By assuming $|\lambda_{\text{SP}}| \gg \sqrt{\epsilon_h}a\omega/c$, we then deduce

$$\frac{1}{\sqrt{\epsilon_h}} \frac{H_{\lambda_{\text{SP}}}^{(1)'}(\sqrt{\epsilon_h}a\omega/c)}{H_{\lambda_{\text{SP}}}^{(1)}(\sqrt{\epsilon_h}a\omega/c)} \sim -\frac{[\lambda_{\text{SP}}^2 - \epsilon_h(a\omega/c)^2]^{1/2}}{\epsilon_h(a\omega/c)}. \quad (32)$$

Eq. (26) can now be solved and we easily find

$$\lambda_{\text{SP}}(\omega) \sim \left(\frac{\omega a}{c}\right) \sqrt{\frac{\epsilon_h \epsilon_c(\omega)}{\epsilon_h + \epsilon_c(\omega)}}. \quad (33)$$

We have obtained an asymptotic expansion for λ_{SP} or more exactly for the real part of λ_{SP} . Indeed, the right-hand side of (33) is purely real. The perturbative resolution of Eq. (26) did not permit us to extract the small imaginary part of λ_{SP} . Of course, it would be possible to improve (33) by taking into account higher orders in the asymptotic expansions (27) and (30). But that does not seem necessary. First, this does not provide an imaginary part for λ_{SP} . In fact, as we shall see below, this term corresponds to an exponentially small contribution which lies beyond all orders in perturbation theory. Furthermore, we have numerically tested the formula (33) for various values of the parameters ϵ_{∞} , ϵ_h , ω_p , ω_T or ω_L . In all cases, it provides a rather good approximation for $\text{Re } \lambda_{\text{SP}}$ (see, for example, Figs. 8 and 9 for the two configurations previously studied). It should be noted that it also predicts the divergence of $\text{Re } \lambda_{\text{SP}}$ for $\omega \rightarrow \omega_s$.

We can now insert (33) into (22). The contributions corresponding to the SP propagating counterclockwise and clockwise are then given by

$$\exp[i(\pm\lambda_{\text{SP}}(\omega)\theta - \omega t)] = \exp[i(\pm k_{\text{SP}}(\omega)a\theta - \omega t)] \quad (34)$$

with

$$k_{\text{SP}}(\omega) = \left(\frac{\omega}{c}\right) \sqrt{\frac{\epsilon_h \epsilon_c(\omega)}{\epsilon_h + \epsilon_c(\omega)}}. \quad (35)$$

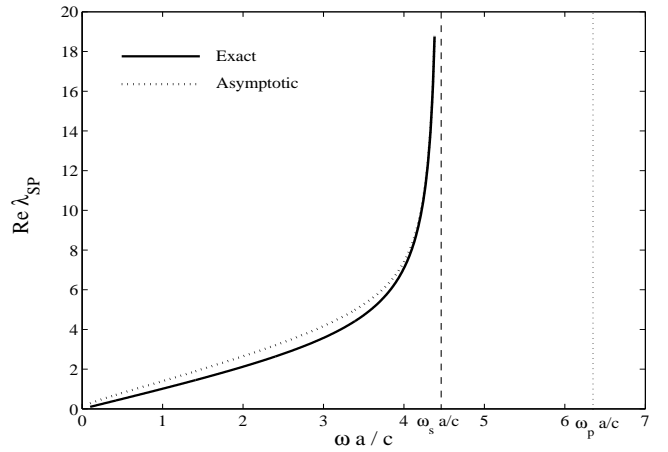


FIG. 8: Regge trajectory for the SP Regge pole. Comparison between exact and asymptotic theories. $\epsilon_c(\omega)$ has the Drude type behavior with $\epsilon_{\infty} = 1$ and $\omega_p a/c = 2\pi$ while $\epsilon_h = 1$.

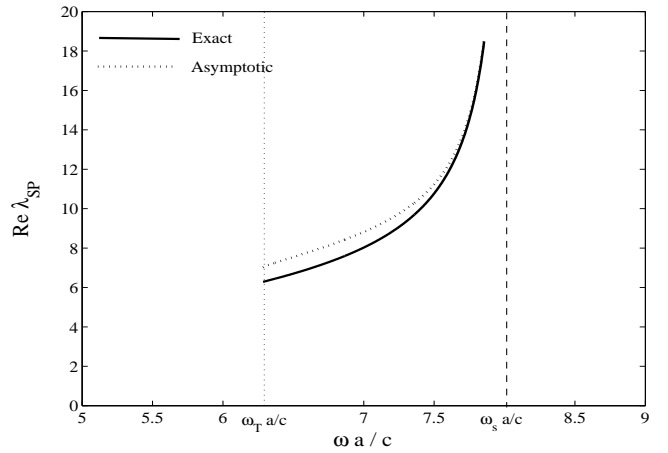


FIG. 9: Regge trajectory for the SP Regge pole. Comparison between exact and asymptotic theories. $\epsilon_c(\omega)$ has the ionic crystal behavior with $\epsilon_{\infty} = 1$, $\omega_T a/c = 2\pi$ and $\omega_L a/c = 3\pi$ while $\epsilon_h = 1$.

Here we have reintroduced the time dependence $\exp(-i\omega t)$ in order to clarify the physical interpretation. From (34) and by noting that $a d\theta$ represents the length element on the cylinder surface, it now appears that the SP propagation is supported by the cylinder surface which thus plays the role of a Bohr-Sommerfeld-type orbit and that (35) can be considered as the SP dispersion relation. This relation could permit us to derive analytically the phase velocity $v_p = \omega/k_{\text{SP}}(\omega)$ as well as the group velocity $v_g = d\omega/dk_{\text{SP}}(\omega)$ of the SP.

It should be also noted that the dispersion relation (35) is in fact the usual dispersion relation of a SP supported by a flat metal-dielectric or semiconductor-dielectric interface (see, for example Ref. 32). We have recovered the same dispersion relation because we have limited the perturbative resolution of Eq. (26) to the lowest order. By taking into account higher orders in the asymptotic

expansions (27) and (30), we could obtain corrections for (33) and (35) vanishing for $a \rightarrow \infty$, i.e. in the limit of large radius.

By inserting the expression (33) for $\lambda_{\text{SP}}(\omega)$ into the Bohr-Sommerfeld quantization condition (23), we can de-

rive approximations for the resonance excitation frequencies $\omega_{\ell\text{SP}}^{(o)}$. If the dielectric function of the cylinder is given by (2), we obtain for the reduced frequencies

$$\frac{\omega_{\ell\text{SP}}^{(o)} a}{c} \approx \frac{1}{\sqrt{2}} \left[\left(\frac{\omega_p a}{c} \right)^2 + \left(\frac{\epsilon_h + \epsilon_\infty}{\epsilon_h \epsilon_\infty} \right) \ell^2 - \sqrt{\left[\left(\frac{\omega_p a}{c} \right)^2 + \left(\frac{\epsilon_h + \epsilon_\infty}{\epsilon_h \epsilon_\infty} \right) \ell^2 \right]^2 - \frac{4}{\epsilon_h} \left(\frac{\omega_p a}{c} \right)^2 \ell^2} \right]^{1/2}. \quad (36)$$

This analytic formula provides accurate results for “large” values of ℓ . For $\ell = 3$, the error is around 13 % and it becomes less than 1 % for $\ell > 7$. Furthermore, it predicts the convergence to $\omega_s = \omega_p / \sqrt{1 + \epsilon_h / \epsilon_\infty}$ when $\ell \rightarrow \infty$. For the dielectric function (3), we obtain

$$\frac{\omega_{\ell\text{SP}}^{(o)} a}{c} \approx \frac{1}{\sqrt{2}} \left[\left(\frac{\omega_L a}{c} \right)^2 + \left(\frac{\epsilon_h + \epsilon_\infty}{\epsilon_h \epsilon_\infty} \right) \ell^2 - \sqrt{\left[\left(\frac{\omega_L a}{c} \right)^2 + \left(\frac{\epsilon_h + \epsilon_\infty}{\epsilon_h \epsilon_\infty} \right) \ell^2 \right]^2 - \frac{4}{\epsilon_h \epsilon_\infty} \left[\epsilon_\infty \left(\frac{\omega_L a}{c} \right)^2 + \epsilon_h \left(\frac{\omega_T a}{c} \right)^2 \right] \ell^2} \right]^{1/2}. \quad (37)$$

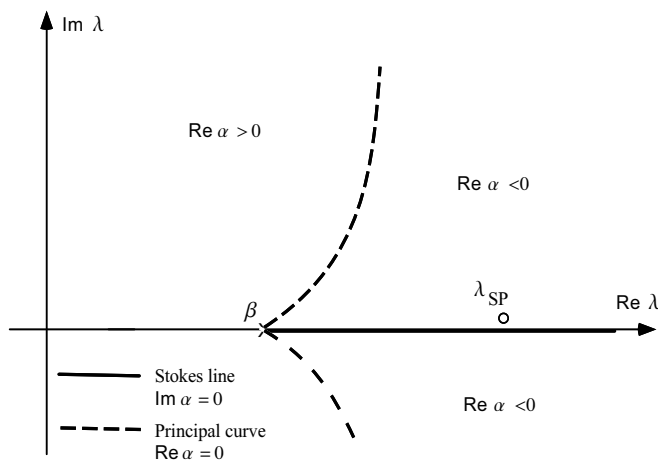


FIG. 10: The relative positions, in the λ -complex plane, of the Regge pole λ_{SP} and the reduced frequency $\beta = \sqrt{\epsilon_h} \omega a / c$.

This analytic formula provides accurate results for “large” values of ℓ . For $\ell = 7$, the error is around 3 % and it becomes less than 1 % for $\ell > 10$. Furthermore, it predicts the accumulation of resonances at $\omega_s = \sqrt{(\omega_L^2 + (\epsilon_h / \epsilon_\infty) \omega_T^2) / (1 + \epsilon_h / \epsilon_\infty)}$ for $\ell \rightarrow \infty$.

To conclude this section, we shall come back to the damping constant $\text{Im } \lambda_{\text{SP}}(\omega)$ of the SP. Numerically (see Figs. 6 and 7) we have shown that this term is small but we cannot consider that it vanishes as we previously found. In fact, this term corresponds to an exponentially small contribution which lies beyond all orders of the asymptotic expansion (30) and which can be captured by

carefully taking into account Stokes’ phenomenon^{33,34}. (For modern aspects of asymptotics beyond all orders and of Stokes’ phenomenon, we refer to a beautiful article by Berry³⁵ as well as to Refs. 36,37,38). Instead of (30), we shall use the Debye asymptotic expansion of $H_\lambda^{(1)}(z)$ in the form

$$H_\lambda^{(1)}(z) \sim -iA(\lambda, z)e^{-\alpha(\lambda, z)}(1 + \dots) + S[\alpha(\lambda, z)]A(\lambda, z)(1 + \dots)e^{\alpha(\lambda, z)}. \quad (38)$$

In the right-hand side of (38), the first term is the usual Debye asymptotic expansion truncated near its least term. The second one is obtained by decoding the divergent tail of that asymptotic expansion. This can be done (see Refs. 35,38) by Borel summation after exploiting a resurgence formula discovered by Dingle³⁶. In the region of the λ -complex plane where the Regge pole λ_{SP} lies (see Fig. 10), we have $\text{Re } \alpha < 0$. As a consequence, the first term of the right-hand side of (38) is the dominant contribution while the second one is a subdominant term which can be forgotten when $|\lambda| \rightarrow \infty$. That is what we did previously by using (30). The Stokes multiplier function $S[\alpha(\lambda, z)]$ is a complicated function involving the exponential integral function E_1 . It goes continuously from 0 to 1 at the crossing of the Stokes line $\text{Im } \alpha = 0$ emerging from the turning point $z = \beta$ (see Fig. 10). Below the Stokes line, it rapidly vanishes. On the Stokes line, it is equal to 1/2 and above the Stokes line it rapidly becomes equal to 1. It thus describes the rapid but continuous birth of the subdominant contribution near the Stokes line.

From (38) we can now write

$$\frac{1}{\sqrt{\epsilon_h}} \frac{H_{\lambda_{\text{SP}}}^{(1)' }(\sqrt{\epsilon_h} a \omega / c)}{H_{\lambda_{\text{SP}}}^{(1)}(\sqrt{\epsilon_h} a \omega / c)} \sim - \frac{[\lambda_{\text{SP}}^2 - \epsilon_h (a \omega / c)^2]^{1/2}}{\epsilon_h (a \omega / c)} \times \left(1 - 2iS[\alpha(\lambda_{\text{SP}}, \sqrt{\epsilon_h} a \omega / c)] e^{2\alpha(\lambda_{\text{SP}}, \sqrt{\epsilon_h} a \omega / c)} \right) \quad (39)$$

instead of (32). By using (29) and (39), Eq. (26) can be solved approximately and we find

$$\text{Re } \lambda_{\text{SP}}(\omega) \sim \left(\frac{\omega a}{c} \right) \sqrt{\frac{\epsilon_h \epsilon_c(\omega)}{\epsilon_h + \epsilon_c(\omega)}}, \quad (40a)$$

$$\text{Im } \lambda_{\text{SP}}(\omega) \sim 2 \left(\frac{\omega a}{c} \right) P(\omega) S(\omega) e^{2\alpha(\omega)} \quad (40b)$$

where

$$P(\omega) \approx \frac{\epsilon_h^2 \epsilon_c^2(\omega)}{(\epsilon_h^2 - \epsilon_c^2(\omega)) \sqrt{\epsilon_h \epsilon_c(\omega) (\epsilon_h + \epsilon_c(\omega))}}, \quad (41a)$$

$$\alpha(\omega) \approx \alpha \left(\left(\omega a / c \right) \sqrt{\frac{\epsilon_h \epsilon_c(\omega)}{\epsilon_h + \epsilon_c(\omega)}}, \sqrt{\epsilon_h} a \omega / c \right), \quad (41b)$$

$$S(\omega) \approx S \left[\alpha \left(\left(\omega a / c \right) \sqrt{\frac{\epsilon_h \epsilon_c(\omega)}{\epsilon_h + \epsilon_c(\omega)}}, \sqrt{\epsilon_h} a \omega / c \right) \right]. \quad (41c)$$

We can see easily that the imaginary part (40b) of λ_{SP} vanishes for $\omega = \omega_s$ as well as in the large radius limit $a \rightarrow \infty$, i.e. in the flat interface limit. Furthermore, we have numerically studied (40b) for “high” values of ω , i.e. when the Regge pole λ_{SP} is very close to the Stokes line. In that case, by giving to the Stokes multiplier function S the value 1/2, we have checked that (40b) provides accurate results for the imaginary part of λ_{SP} . We therefore consider we have succeeded in providing an analytic formula for the Regge pole of the SP. However, the expression (40b) is a rather complicated function of ω . As a consequence, its use in the semiclassical formula (25) is unfortunately not very interesting. In short, we think that (40b) is especially interesting for the qualitative description of the SP damping it provides.

V. CONCLUSION AND PERSPECTIVES

In this article we have introduced the CAM method in the context of scattering of electromagnetic waves from metallic and semiconducting cylinders. This allows us to provide a physical explanation for the excitation mechanism of RSPM’s as well as a simple mathematical description of the surface wave (i.e. the SP) that generates them. It should be noted that our results are not limited to metals and semiconductors. Under simple assumptions, they are also valid, *mutatis mutandis*, for more general materials. Indeed, in a frequency range where

the dielectric function of a material presents a dominant simple pole ω_o , it is always possible to write²⁷

$$\epsilon_c(\omega) \approx \epsilon_\infty + \frac{2\omega_o R}{\omega_o^2 - \omega(\omega + i\gamma)}. \quad (42)$$

Here ω_o is the resonance frequency of the material in the frequency region considered, γ denotes the associated damping term, ϵ_∞ stands for the high-frequency limit of the dielectric function and we assume that the coefficient R is positive. In the absence of dissipation ($\gamma \approx 0$) and if the zero of $\epsilon_c(\omega)$ which is given by $\sqrt{\omega_o^2 + 2\omega_o R / \epsilon_\infty}$ lies in the validity range of Eq. (42), there exists a SP which can be described by the theory developed in Sections 3 and 4.

In parallel with the semiclassical analysis of SP’s on metallic or semiconducting cylinders, we have developed a new picture of the photon-cylinder system: it can be viewed as an artificial atom for which the photon plays the role of an electron. RSPM’s are long-lived quasi-bound states for this atom, the associated complex frequencies are Breit-Wigner-type resonances while the trajectory of the SP which generates them is a Bohr-Sommerfeld-type orbit. Furthermore, the imaginary part of a given RSPM complex frequency corresponds to an exponentially small term which lies beyond all orders in perturbation theory. As a consequence, as their excitation frequency increases, RSPM’s gain very long lifetimes, i.e. they behave like bound states.

With in mind applications in photonic crystal physics, our work could be naturally extended in various directions including i) scattering by cylinders with metallic or semiconducting coating, or more generally, multilayered structures, ii) scattering by metallic or semiconducting spheres and last but not least iii) scattering by objects fabricated from left-handed materials. It would be also interesting to provide a complete (i.e., not limited to SP’s) semiclassical description of scattering of electromagnetic waves from metallic and semiconducting objects in the framework of CAM techniques by extending the ideas of Nussenzveig and coworkers²⁰. But at first sight that seems to be a formidable task.

In recent papers dealing with photonic band structure of two-dimensional photonic crystals fabricated from metallic or semiconducting cylinders arrayed in a square lattice, a striking feature has been noted^{1,5,8,9,10,11,12,13}, namely the existence of flat bands (i.e. dispersionless bands) in the frequency range in which $\epsilon(\omega) < 0$. This result, which only exists for H polarization, is of course linked to the excitation of RSPM’s. More precisely, it is due to the localization of the photon which is trapped on the Bohr-Sommerfeld orbit. Of course, this analysis is rather over-simplified. In fact, it is necessary to understand up to what point single-cylinder resonant aspects are related to “resonant” aspects of the full photonic crystal. Recently, Ito and Sakoda^{4,11} have considered this problem by developing a physically intuitive but appealing analysis: they regard the RSPM’s of an isolated cylinder as atomic orbitals and they describe their

effects into the photonic crystal in the context of the “linear combination of atomic orbitals (LCAO) theory”. Ito and Sakoda do not use the terminology “artificial atom” to describe the photon-cylinder system but this picture is implicitly present in their work and the point of view we develop in the present article strengthens their analysis.

Of course, it should be interesting to provide a more rigorous interpretation of the existence of the flat bands. With this aim in view, it would be possible to benefit from the machinery developed in semiclassical physics (see, for example, Ref. 39 and references therein) to analyze quantum chaos in connection with multiple scattering. As far as we know, such a semiclassical approach has never been considered in the context of photonic crystal physics but it seems to us very promising. Indeed, it is well-known that, due to convergence problems,

band structure computations of metallic or semiconducting photonic crystals are very heavy in the frequency range in which $\epsilon(\omega) < 0$. The semiclassical approach could permit us to easily construct these band structures by taking into account the shortest periodic orbits involving SP trajectories and lying into the Wigner-Seitz cell. Here, the properties we have found for the SP would be very useful.

Acknowledgments

We are grateful to Nick Halmagyi for help with English.

-
- * Electronic address: ancey@univ-corse.fr
 † Electronic address: decanini@univ-corse.fr
 ‡ Electronic address: folacci@univ-corse.fr
 § Electronic address: gabrieli@univ-corse.fr
- ¹ A. R. McGurn and A. A. Maradudin, Phys. Rev. B **48**, 17576 (1993).
 - ² J. D. Joannopoulos, R. D. Mead, and J. N. Winn, *Photonic Crystals* (Princeton University Press, Princeton, 1995).
 - ³ S. G. Johnson and J. D. Joannopoulos, *Photonic Crystals: The Road from Theory to Practice* (Kluwer Academic Publishers, Boston, 2001).
 - ⁴ K. Sakoda, *Optical Properties of Photonic Crystals* (Springer-Verlag, Berlin, 2001).
 - ⁵ V. Kuzmiak, A. A. Maradudin, and F. Pincemin, Phys. Rev. B **50**, 16835 (1994).
 - ⁶ M. M. Sigalas, C. T. Chan, K. M. Ho, and C. M. Soukoulis, Phys. Rev. B **52**, 11744 (1995).
 - ⁷ W. Zhang, A. Hu, X. Lei, N. Xu, and N. Ming, Phys. Rev. B **54**, 10280 (1996).
 - ⁸ V. Kuzmiak, A. A. Maradudin, and A. R. McGurn, Phys. Rev. B **55**, 4298 (1997).
 - ⁹ V. Kuzmiak and A. A. Maradudin, Phys. Rev. B **55**, 7427 (1997).
 - ¹⁰ H. van der Lem and A. Moroz, J. Opt. A: Pure Appl. Opt. **2**, 395 (2000).
 - ¹¹ T. Ito and K. Sakoda, Phys. Rev. B **64**, 045117 (2001).
 - ¹² E. Moreno, D. Erni, and C. Hafner, Phys. Rev. B **65**, 155120 (2002).
 - ¹³ T. Ochiai and J. Sanchez-Dehesa, Phys. Rev. B **65**, 245111 (2002).
 - ¹⁴ R. Englman and R. Ruppin, J. Phys. C **1**, 1515 (1968).
 - ¹⁵ C. A. Pfeiffer, E. N. Economou, and K. L. Ngai, Phys. Rev. B **10**, 3038 (1974).
 - ¹⁶ J. C. Ashley and L. C. Emerson, Surf. Sci. **41**, 615 (1974).
 - ¹⁷ S. S. Martinos and E. N. Economou, Phys. Rev. B **28**, 3173 (1983).
 - ¹⁸ G. N. Watson, Proc. Roy. Soc. London A **100**, 83 (1918).
 - ¹⁹ R. G. Newton, *Scattering Theory of Waves and Particles* (Springer-Verlag, New-York, 1982), 2nd ed.
 - ²⁰ H. M. Nussenzweig, *Diffraction Effects in Semiclassical Scattering* (Cambridge University Press, Cambridge, 1992).
 - ²¹ J. W. T. Grandy, *Scattering of Waves from Large Spheres* (Cambridge University Press, Cambridge, 2000).
 - ²² N. Andersson and K.-E. Thylwe, Class. Quantum Grav. **11**, 2991 (1994).
 - ²³ N. Andersson, Class. Quantum Grav. **11**, 3003 (1994).
 - ²⁴ Y. Décanini, A. Folacci, and B. P. Jensen, Phys. Rev. D **67**, 124017 (2003).
 - ²⁵ Y. Décanini and A. Folacci, Phys. Rev. A **67**, 042704 (2003).
 - ²⁶ N. W. Ashcroft and N. D. Mermin, *Solid State Physics* (Saunders College Publishing, Philadelphia, 1976).
 - ²⁷ M. Fox, *Optical Properties of Solids* (Oxford University Press, Oxford, 2001).
 - ²⁸ N. F. Mott and H. S. W. Massey, *The Theory of Atomic Collisions* (Oxford University Press, Oxford, 1965).
 - ²⁹ M. Abramowitz and I. A. Stegun, *Handbook of Mathematical Functions* (Dover, New-York, 1965).
 - ³⁰ G. N. Watson, *Theory of Bessel Functions* (Cambridge University Press, Cambridge, 1995), 2nd ed.
 - ³¹ H. M. Nussenzweig, Ann. Phys. (N.Y.) **34**, 23 (1965).
 - ³² H. Raether, *Surface Plasmons* Vol. 111 of Springer Tracts in Modern Physics (Springer-Verlag, Berlin, 1988).
 - ³³ G. G. Stokes, Trans. Camb. Phil. Soc. **9**, 379 (1847).
 - ³⁴ G. G. Stokes, Trans. Camb. Phil. Soc. **10**, 106 (1864).
 - ³⁵ M. V. Berry, Proc. R. Soc. London **A 422**, 7 (1989).
 - ³⁶ R. D. Dingle, *Asymptotic Expansions: Their Derivation and Interpretation* (Academic Press, London, 1973).
 - ³⁷ H. Segur, S. Tanveer, and H. Levine, *Asymptotics Beyond all Orders* (Plenum, New York, 1991).
 - ³⁸ M. V. Berry and C. J. Howls, Proc. R. Soc. London **A 430**, 653 (1990).
 - ³⁹ M. Brack and R. K. Bhaduri, *Semiclassical Physics* (Addison-Wesley, Reading, 1997).